Desalination and Water Treatment
www.deswater.com

doi: 10.5004/dwt.2018.21984

105 (2018) 298–309
February

Preparation of magnesium silicate/polyethersulfone hybrid ultrafiltration membrane for macromolecular intercept and dye removal

Senjian Han, Lili Mao, Haizeng Wang*

Key Laboratory of Marine Chemistry Theory and Technology, Ministry of Education, College of Chemistry and Chemical Engineering, Ocean University of China, Qingdao, Shandong 266100, China, Tel. +86 532 66782503, Fax +86 532 66782481, email: senjianhan@163.com (S. Han), maolili@ouc.edu.cn (L. Mao), haizwang@ouc.edu.cn (H. Wang)

Received 24 August 2017; Accepted 1 February 2018

ABSTRACT

Magnesium silicate (MgSiO)/polyethersulfone (PES) hybrid membranes were prepared by phase inversion method, in which MgSiO particles were in-situ synthesized during the formation of membrane. Energy dispersive X-ray spectrometry (EDS), scanning electron microscopy (SEM) and atomic force microscope (AFM) measurements were performed to characterize the component and morphology of membranes, while X-ray diffraction (XRD) and Fourier transform-infrared spectroscopy (FT-IR) were conducted to characterize MgSiO particles morphology as well as its structural properties and the presence of functional groups. What's more, the properties of membranes were investigated. Results showed that MgSiO particles were formed in a Mg/Si ratio of 1.36, and dispersed uniformly both on the membrane surface as well as matrix. The porosity and permeation of hybrid membranes were found a decrease and then an overall increase, along with the increased MgSiO content. Compared with the PES membrane, the hydrophilicity, separation performance and antifouling property of the hybrid membranes were enhanced due to the existence of MgSiO. Moreover, the hybrid membranes present both a higher BSA (bovine serum albumen) rejection, and a higher rejection towards MB (methylene blue) solution.

Keywords: Magnesium silicate; Hybrid membrane; Hydrophilicity; BSA rejection; MB removal

1. Introduction

The discharge of organic pollutants into natural waters without proper treatment has caused severe water pollution [1]. Up to now, a number of technologies have been adopted to control water pollution, focusing on water purification, such as distillation, photocatalyst, adsorption, electrochemical, membrane filtration, etc. [2–10] Among these, membrane technology is becoming increasingly important as an efficient technology to solve problems of polluted water or to recycle valuable compounds in several processes [11,12].

As a non-negligible technology, ultrafiltration is one type of the membrane technology, used in paint recovery, protein separation and water treatment for pre-filtration in reverse osmosis [13,14]. As a commonly used ultrafiltration membrane material, polyethersulfone (PES) exhibits good thermal, hydrolytic stability as well as good mechanical and membrane forming properties [15]. However, pure polymer PES is quite hydrophobic. As a consequence, the addition of inorganic additive into the polymer has then become an efficient technique for membrane hydrophilicity modification, to increase water permeability and lower the membrane fouling [16].

Organic–inorganic membranes prepared by the addition of inorganic additive into polymer membrane matrix exhibits characteristics of both in organic material and organic polymer [17]. Most commonly, the preparation method can be divided into solution blending method, in-situ polymerization and sol-gel method [18]. Much effort has been done towards method improvement to promote the dispersion of inorganic additives [19–21]. With the same consideration, the in-situ synthesized phase inversion method was devel-

*Corresponding author.

oped in our previous study, which realized the inorganic additive uniform dispersion [22].

Usually, the ultrafiltration membrane, based on size exclusion or particle capture, is used generally to remove particulates and macromolecules, which basically has no efficient rejection on micromolecule dye [23,24]. Although nanofiltration membrane has smaller pore size, recognized as one of the best available techniques for the removal of several toxic dyes, which is not comparable to ultrafiltration membrane in high permeability and low cost [25]. It is supposed that a ultrafiltration membrane with good performance and possessing high rejection towards dye is meaningful to be found out.

Based on this purpose, magnesium silicate was chosen as the additive synthesized in polymer PES to form hybrid ultrafiltration membrane. As a kind of inorganic material, magnesium silicate, composed of free silanol groups, provides not only the hydrophilic groups but also active sites for adsorption of organic particles[26]. It has particular use in color removal [26–29]. To our knowledge, there has no report on magnesium silicate hybrid membrane as a separation membrane. Meanwhile, the magnesium silicate ultrafiltation membrane has its unique properties on removal of monomolecular dyes, showing part of the performance of nanofiltration membrane.

Applying the previous developed in-situ synthesized phase inversion method in the present study, precursor magnesium salt was dissolved into the casting solution, reacted with Na_2SiO_3 in the coagulation bath. Magnesium silicate was synthesized during the process of membrane formation and dispersed uniformly in the PES membrane matrix. The prepared membranes were characterized by EDS, SEM, AFM and BET. Subsequently, magnesium silicate particles separated from the dissolved hybrid membranes were characterized by XRD and FT-IR. Additionally, the pure water flux, BSA (bovine serum albumen) rejection and antifouling performance were investigated and compared in detail. Furthermore, BSA static adsorption and MB (methylene blue) dynamic intercept tests have been examined.

2. Experimental

2.1. Materials

Polyethersulfone (PES, MW = 58,000 Da) was purchased from BASF (Qingdao, China), and polyethylene glycol (PEG Mw = 400 g/mol) was purchased from Shanpu Co. Ltd. (Shanghai). N,N-dimethylacetamide (DMAc) was purchased from Guangchen Chemical Reagent Co. Ltd. (Tianjin), and bovine serumalbumin (BSA Mw = 67 kDa) was purchased from Zhengjiang High-technology Co. Ltd. (Tianjin). Both sodium silcate ($Na_2SiO_3·9H_2O$) and magnesium chloride hexahydrate ($MgCl_2·6H_2O$) were purchased from Sinopharm Chemical Reagent Co., Ltd. All reagents were of regent grade and used without further purification.

2.2. Membrane preparation

PES was added to DMAc containing PEG and $MgCl_2·6H_2O$, followed by sonicating for 0.5 hour and full stirring at 70°C overnight. The resulted homogenous solution was rested at room temperature until no bubbles were observed, and then cast on a clean plate with a casting knife of 200 μm. After a 30 s exposure to air, the cast film was immediately immersed in Na_2SiO_3 (0.5 mol/L) bath. After complete coagulation, the membranes were washed with DI water until the cleaning solution was neutral and the residual solvent was removed.

With the dosage of $MgCl_2·6H_2O$ changing in the casting solution, the obtained membranes were named, and the details were described in Table 1.

2.3. Membrane characterization

2.3.1. Microscopy analysis

The membrane surface and cross-sectional morphology were observed by scanning electron microscopy (SEM, S-4800, Hitachi, Japan). And the EDS-system (EX-250, HORIBA, Japan) was coupled with SEM to study the chemical elements of interest in the membranes. After cutting into appropriate size, the membrane samples were mounted on sample stage, and gold sputtered before analyzing. Additionally, in order to analyze cross-sectional morphology, the membrane samples should be fractured in liquid nitrogen.

The membrane surface roughness was analyzed by atomic force microscope (AFM, Nano 3D, Veeco, USA). A membrane sample, approximately 1 cm^2, was fixed on a metal support and the surface was imaged in a scan size of 2 μm × 2 μm. The mean roughness (R_a) and the root mean square of the Z data (R_{ms}) were calculated from the topography scans.

2.3.2. Characterization of magnesium silicate

In order to confirm the chemical components of the newly generated particles, the hybrid membrane was dissolved in DMAc, the solvent also used in casting solution. Unlike the original pellucid casting solution, the obtained solution was turbid, which was mostly caused by the newly generated insoluble particles. Next, precipitates separate from the liquid by a centrifuge, which were then washed and dried. The gained particles was tested by X-ray diffraction (XRD) using 18 kW CuKα radiation and Fourier transform infrared (FT-IR, Tensor27, BRUKER, Germany) spectra analysis.

Table 1
The casting solution composition with different amount of $MgCl_2·6H_2O$

Sample	Casting solution compositions (wt.%)			$MgCl_2·6H_2O$:PES(w/w)
	PES	DMAc	PEG 400	
M0	18	78	4	0
M1	18	78	4	0.04
M2	18	78	4	0.08
M3	18	78	4	0.12
M4	18	78	4	0.16
M5	18	78	4	0.20

2.3.3. Hydrophilicity measurements

Represented by contact angle, the hydrophilicity of membrane surface was measured by a contact angle meter (DSA100, Kruss, Germany). 5 μL of DI water pumping out from the micro syringe, dropped onto the membrane surface. The instant image was recorded, and the value was calculated. For each membrane sample, the contact angle was measured for more than 10 times, and the average value was reported.

2.3.4 Pore data

The porosity of the prepared membranes, represented by the volume percentage of occupied water, was measured by gravimetric method. The membrane sample with a certain size was wiped the surface water, and weighted quickly (W_w). Then, the weighted membrane was weighted (W_d) again after drying 24 h in a vacuum oven at 60°C. The porosity (P) was calculated as follows:

$$P(\%) = \frac{\frac{W_w - W_d}{\rho_w}}{A \times \delta} \times 100 \quad (1)$$

where W_w and W_d are the wet and dry membranes weights (g), respectively. ρ_w is the DI water density (g/cm^3), A is the membrane area (cm^2) and δ is the thickness (cm).

Other relative parameters, including pore size distribution and surface area were investigated by BET (Brunauer, Emmett, and Teller) analysis using specific surface area analyzer (NOVA 2200e, Quantachrome, USA).

2.3.5. Pure water flux

The membrane sample with an effective area of 19.63 cm^2 was mounted in a self-made filtration apparatus, pre-compacted with DI water at 0.2 MPa for 1 h. Until a steady permeation was reached, the permeated flux was recorded at 0.1 MPa over a period of time. The equation of pure water flux (J_w) is as follows:

$$J_{w1} = \frac{Q}{A\Delta t \Delta p} \quad (2)$$

where Q is the permeate water volume (L), A is the effective membrane area (m^2), Δt is the collection time (h), and Δp is the trans-membrane pressure (MPa). All the J_{w1} (L/m^{2}h Pa) is calculated three times, and the reported data presents an average value.

2.3.6. Separation and antifouling performance

After recording the pure water permeability, the membranes were subject to 1 g/L bovine serum albumin (BSA, 67 kDa) solution, prepared with phosphate buffered solution (pH = 7). Both solutions in feed and permeate were evaluated by a UV-vis spectrophotometer (UV-2450, Shimadzu, Japan) at the maximum absorption wavelength of 280 nm, obtained from Fig. 1a. The rejection rate (R) was calculated using the following equation:

$$R(\%) = \left(1 - \frac{C_p}{C_f}\right) \times 100 \quad (3)$$

where C_p and C_f are the BSA concentrations in permeate and feed, respectively.

Similarly, the membranes were subject to 6 mg/L methelyene blue (MB, 319.86 Da) solution at 0.1 MPa for 90 min. Both solutions in feed and permeate were evaluated at the maximum absorption wavelength of 664 nm, obtained from Fig. 1b.

To investigate the antifouling property of membranes, the BSA fouled membranes were washed with DI water for 20 min repeatedly, and the water flux of cleaned membranes J_{w2} (L/m^{2}h) was measured again. Based on the fluxes of water or BSA permeation, several ratios were defined, including flux recovery ratio (FRR), total flux decline ratio (R_t), reversible flux decline ratio (R_r) and irreversible flux decline ratio (R_{ir}) using the following expression [30]:

$$FRR\% = \frac{J_{w2}}{J_{w1}} \times 100 \quad (4)$$

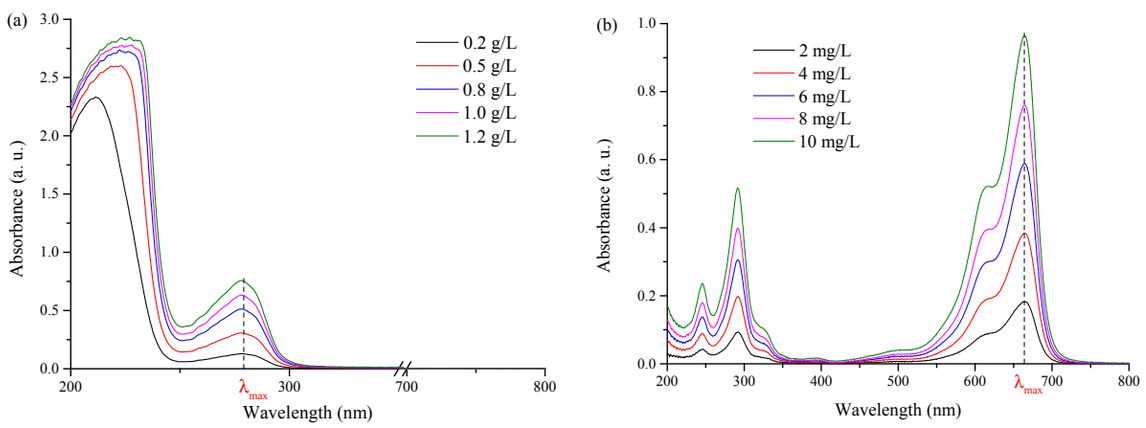

Fig. 1. The adsorption UV-vis spectra of BSA solutions (a) and MB solutions(b).

$$R_t\% = \left(1 - \frac{J_p}{J_{w1}}\right) \times 100 \quad (5)$$

$$R_r\% = \frac{J_{w2} - J_p}{J_{w1}} \times 100 \quad (6)$$

$$R_{ir}\% = \frac{J_{w1} - J_{w2}}{J_{w1}} \times 100 \quad (7)$$

where J_p is the BSA permeation flux, J_{w1} is the initial pure water flux, and J_{w2} is the pure water flux of the cleaned membrane.

2.3.7 Protein adsorption

BSA (about 0.3 g/L) solution was prepared by DI water to carry out the static adsorption of protein on membranes. The membrane samples were cut into small pieces (5 cm × 5 cm) and immersed in the BSA solution in test tubes (each for 50 mL) at 25°C for 8 h to reach adsorption equilibrium, and all of the solutions before and after the BSA dissolution were approximately neutral (ranging from 7.38 to 7.54). The amount of BSA adsorbed on the membrane samples was calculated using initial and final solutions of BSA concentrations.

3. Results and discussion

3.1. Elemental analysis

The energy dispersive X-ray spectroscopy (EDS) was used to determine the major ingredient of the membrane. The energy dispersive X-ray spectroscopy (EDS) was used to determine the major ingredient of the membrane, and the results are shown in Fig. 2 and Table 2. It can be seen that element Mg and Si were successfully reserved in the hybrid membrane, and the percent of O was raised compared with PES membrane. It can be inferred that the most possible pattern of formed inorganic particles was composed by Mg, Si and O, which can be denoted as MgSiO [28,31]. Moreover, the mean ratios of Mg and Si were calculated according to element weight. Each sample was repeated 6 times, and the mean value of Mg/Si ratio (1.36 ± 0.10) was calculated from all the defined samples.

3.2 Characterization of magnesium silicate

Fig. 3 illustrates the FT-IR spectra of magnesium silicate and marks the peak position. The broad band near 3000–3750 cm^{-1} is ascribed to the stretching vibrations of O-H groups. The weak stretch near 3680 cm^{-1} is attributable to Mg-OH, while the split strong adsorptions near 3400 cm^{-1} are ascribed to H-bonding. Another O-H stretching vibration appears at 1632 cm^{-1}. Magnesium silicate shows a very strong adsorption at about 1028 cm^{-1} with shoulder at about 901 cm^{-1}, is assigned to Si-O stretching and bending vibrations, respectively. Nevertheless, the band near 646 cm^{-1} is assigned to Si-O-Mg bonds. In addition, the band near 567 cm^{-1} is attributed to internal deformation of SiO_4 tetrahedra, and the band near 459 cm^{-1} is ascribed to Mg-O stretching [9,26,32–35].

The XRD pattern is presented in Fig. 4. The results manifest that the precipitates are amorphous with low crystallinity. The broad amorphous peaks at 26°, 35° and 60° for the obtained particles were found to be consistent with the XRD pattern of the amorphous magnesium-silicate-hydrate (M-S-H) phase [32,36].

3.3. Morphological study

The morphology of the prepared membranes was carried out by SEM analysis. The cross-section morphology of the membrane M5 is shown in Fig. 5, and the surface images of the prepared membranes are shown in Fig. 6. All the SEM images show that MgSiO particles are distributed uniformly both on the membrane surface and matrix (M1–M5), which coincides with the previous estimate that precursor $MgCl_2{\cdot}6H_2O$ particles were well-dissolved and converted into MgSiO. From Fig. 6, it can be seen that with the increase of $MgCl_2{\cdot}6H_2O$, the pore size was minished from M0 to M2, while enlarged from M2 to M5, and M2 exhibited the minimum aperture. Whilst the amount of MgSiO formed in the membrane surface increased from M0 to M5. In the beginning, the formation of MgSiO resulted to pore (formed by porogen PEG leaching) blocking, and more pores were blocked with the limited increasing MgSiO. Meanwhile, it is suggested that during the process of phase inversion, the formed hydrophilic MgSiO particles have a high tendency to adsorb water, which can provide sites for water penetration and accelerate the shrinkage of polymer phase, resulting to another pores [37,38]. Both the new generated pores and the increased hydrophilicity accelerate water penetration rate afterwards.

Surface roughness is always a considerable characterization for surface properties and membrane performance [39]. Therefore, it is one of the important parameters for indicating membrane performance. Three-dimensional images of three types of membranes are illustrated in Fig. 7. The average surface roughness was measured from the AFM images according to the variation of the mean height, and the corresponding mean roughness value R_a and the root mean square of the Z data R_{ms} were listed in Table 3. All the membranes showed the ridge-and-valley surface morphology, and Fig. 7b and 7c were found to be much rougher than the PES membrane. The R_a and R_{ms} values were increased with the increase content of MgSiO, and the minimum R_a and R_{ms} values of 5.102 and 6.629 were appeared at PES membrane M0. A slight increase was observed until M2. With the continuous increase of MgSiO, it was showed a significant increase both on R_a and R_{ms}, representing an increased roughness. The increased roughness was not favorable to the antifouling tendency, which was referred in the subsequent section.

3.4. Hydrophilicity of membranes

The surface hydrophilicity can be correlated with the good performance of membranes, including high permeability and antifouling property. Infact, MgSiO existed in

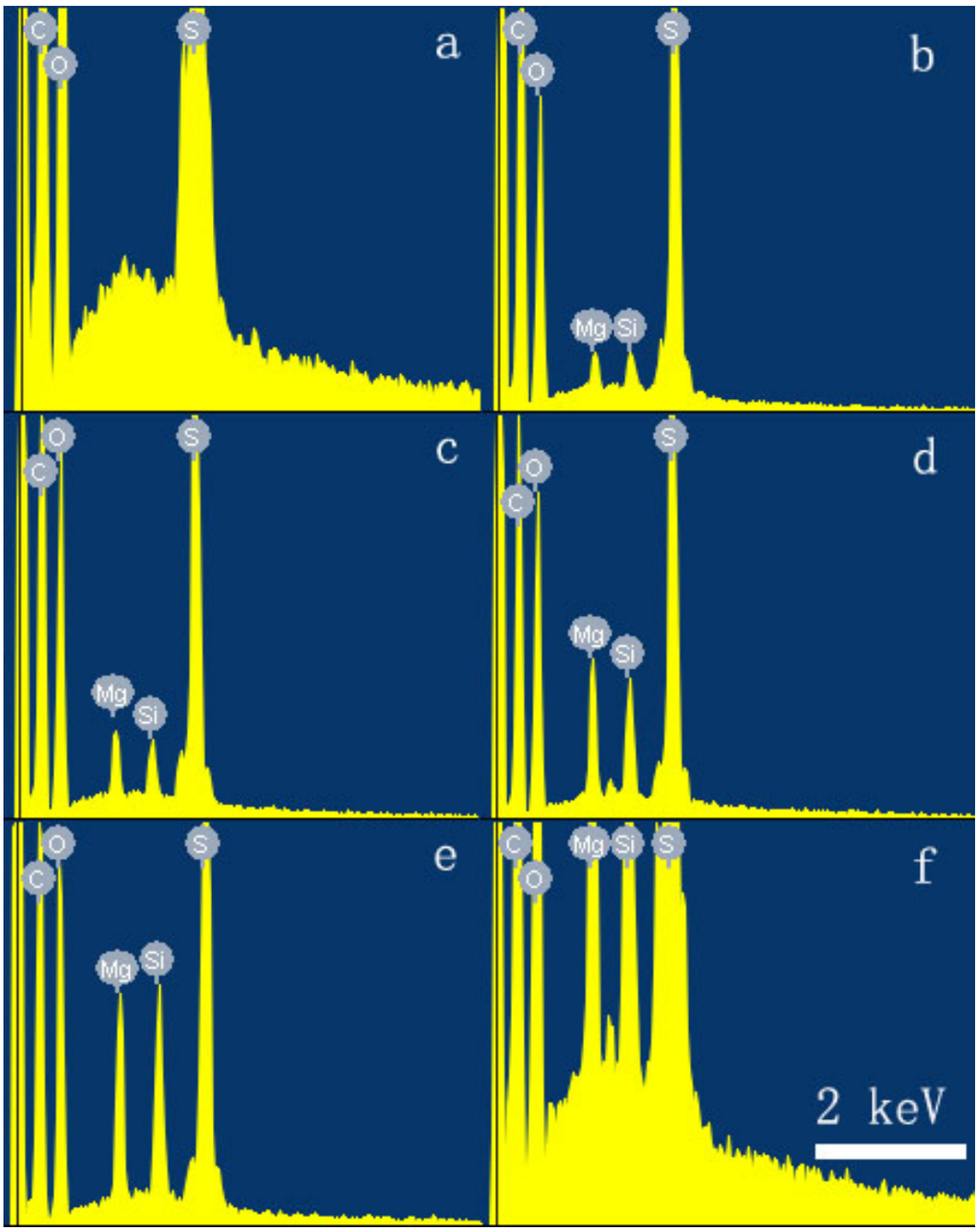

Fig. 2. EDS measurement of the membranes: (a–f) M0–M5.

Table 2
Element weight percent based on EDS analysis

Element	M0	M1	M2	M3	M4	M5
C K	65.76%	62.97%	59.00%	56.01%	57.51%	58.65%
O K	24.12%	27.75%	31.68%	31.52%	30.17%	28.93%
S K	10.12%	8.59%	7.99%	9.50%	8.21%	8.26%
Mg K	0	0.37%	0.75%	1.64%	2.10%	2.23%
Si K	0	0.32%	0.58%	1.33%	2.02%	1.92%

PES membrane surface can improve the hydrophilicity of membrane surface and reduce the water permeation resistance. From Fig. 8 it can be seen that the contact angle value declined sharply (M0 to M1), then it declined gradually (M1 to M4), at last it showed an abnormal rise (M4 to M5). The sharply decline of contact angle was attributed to the existence of MgSiO, consequently the biggest difference appeared between M0 and M1. The continuous decline of contact angle was mainly owed to the enhancement of MgSiO content, providing more Si-OH group in this case. The declined contact angle reflected the enhanced hydro-

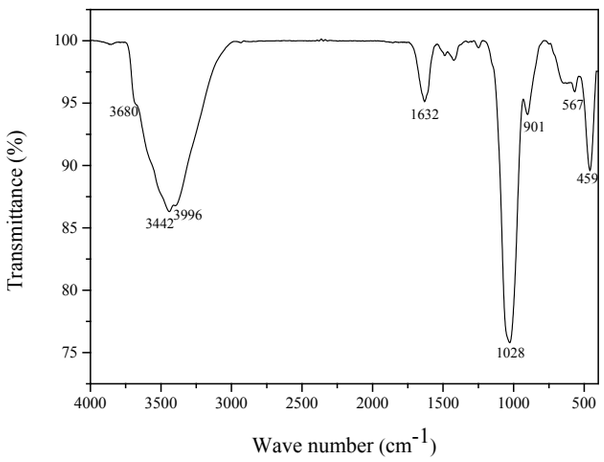

Fig. 3. FT-IR spectrum of the gained particles.

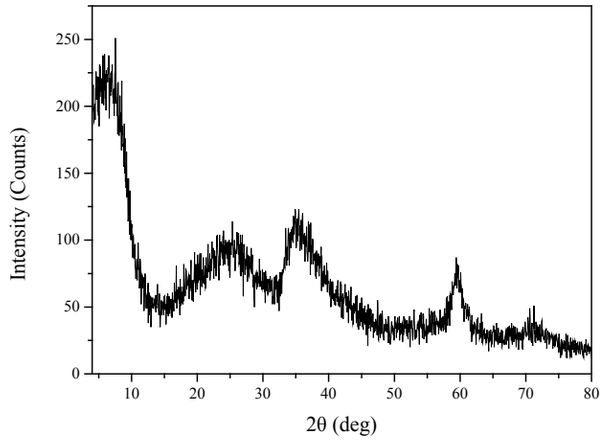

Fig. 4. XRD pattern of magnesium silicate particles.

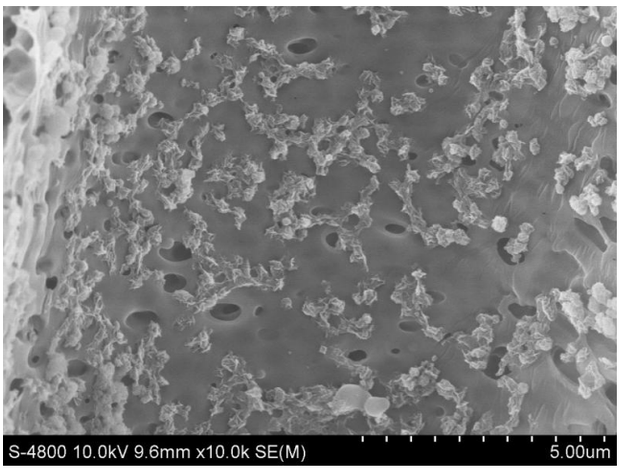

Fig. 5. SEM cross-section image of the generated MgSiO in the membrane M5.

philicity. While the abnormal rise in contact angle possibly can be ignored, this may be affected by the membrane surface roughness [40,41]. From a view of tendency, the addition of MgSiO in PES hybrid membrane improved the surface hydrophilicity.

3.5. Pure water flux and pore data

The permeability property of the prepared membranes was studied at 0.1 MPa by collecting the pure water through a certain time. The obtained values are displayed in Fig. 9, consisting with the trends observed in the SEM images. At the beginning (from M0 to M2) the water flux was decreased sharply, and reached the lowest value at M2, followed by a more and more dramatic increasing. To our knowledge, both the membrane structure and the hydrophilicity have effect on water flux, and the final value depends on the dominating factor [42]. As a pore-forming agent, PEG was added into all casting solutions to generate appropriate pores. However, due to the formation of increasing MgSiO blocking more original pores offset the improved hydrophilicity, the pure water flux was decreased firstly. Whilst the increasing existence of hydrophilic MgSiO not only reduced water permeation resistance but also led to generate new pores, which further accelerate the water permeation, resulting in an increase of water flux.

The result of porosity measurement, also being displayed in Fig. 9, presents the same rule as pure water flux showed, except for M5. The decreased porosity owed to the blocked original pores, while the increased porosity ascribed to the new generated pores. For the membrane M5, it showed lower porosity than M4, which may attributed to more generated pores connected and converted to perforated structure impairing storage water ability of membrane.

To further characterize the nano-scale pore structure of the membrane, the prepared membranes were analyzed by BET analysis. Fig. 10 show the corresponding pores size distribution curves from adsorption branch using BJH method, and Table 4 summarized the data of average pore size and surface area. It can be found that all the pore size distributions of the prepared membranes do not show unimodal distribution, and all the presented extreme values are less than 10 nm. Although there was no significant variation, the average pore diameter also presented increase after the decrease, which confirmed the trend observed by SEM. The BET surface area showed an irregular fluctuation. However, from an overall perspective, the surface area of MgSiO hybrid membrane presented a gradually increasing trend with the increased addition of MgSiO. This may due to the fact that the more inorganic particles formation can cause more pores thereby increasing the BET surface area.

3.6. Separation and antifouling performance of BSA solution

After 0.5 h BSA filtration, the permeate was collected and detected. Repeating three times, the average rejection is shown in Fig. 11. It can be seen that the rejection rate of hybrid membranes (M1 to M5) is higher than the PES membrane (M0). From membrane M0 to M1, an obvious increase in rejection is observed, and for MgSiO hybrid membranes,

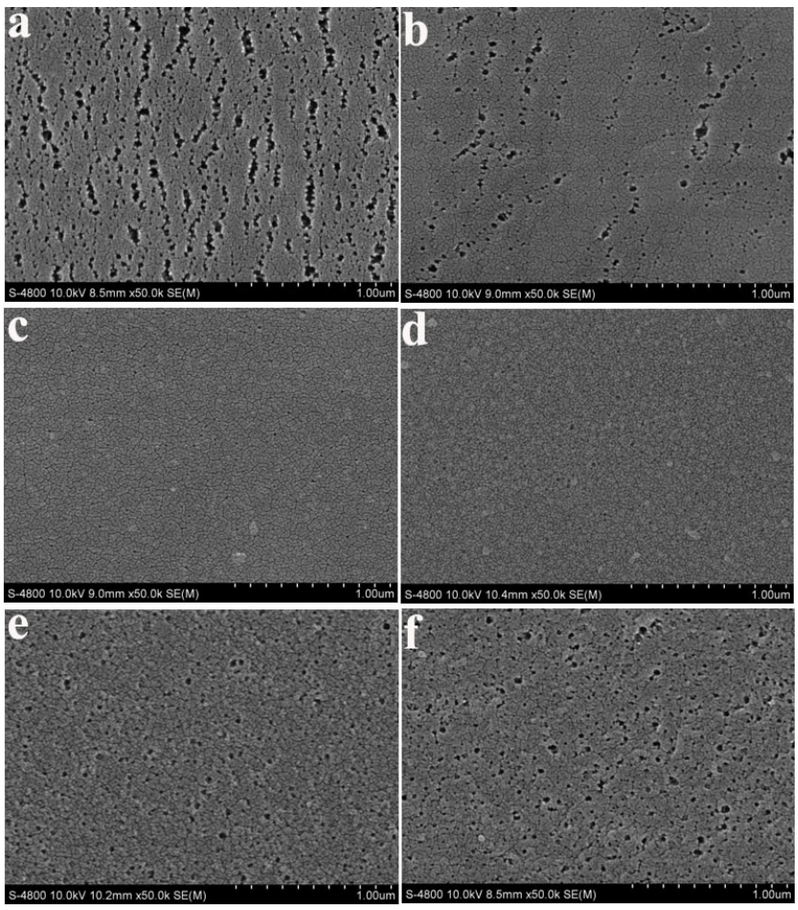

Fig. 6. SEM surface images of the membrane: (a–f) M0–M5.

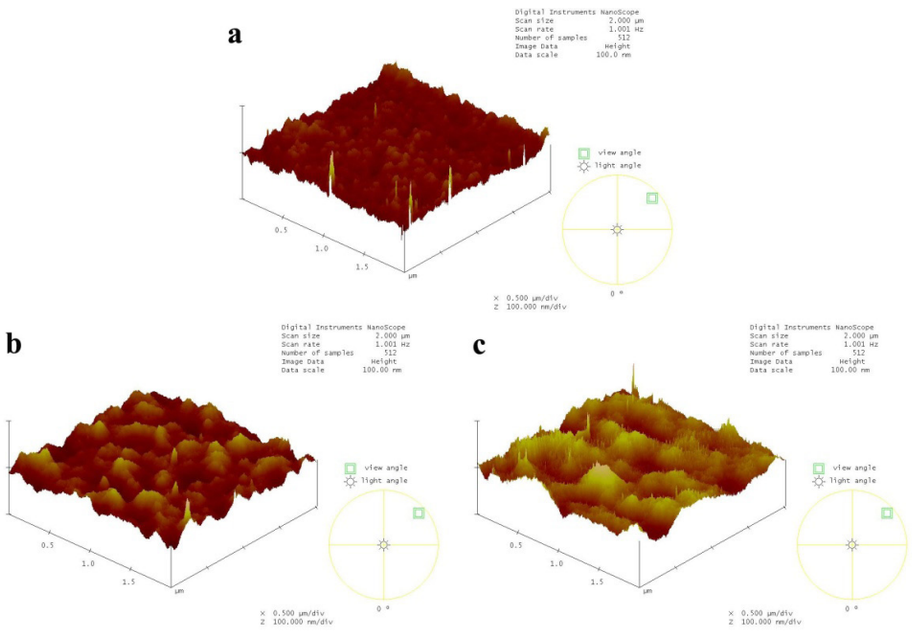

Fig. 7. AFM images of the membranes: (a) M0 (b) M3 (c) M5.

Table3
Surface roughness of the membranes

Roughness parameters	R_a (nm)	R_{ms} (nm)
M0	5.102	6.629
M1	5.167	6.702
M2	5.664	7.131
M3	7.657	9.543
M4	7.823	9.943
M5	8.011	10.331

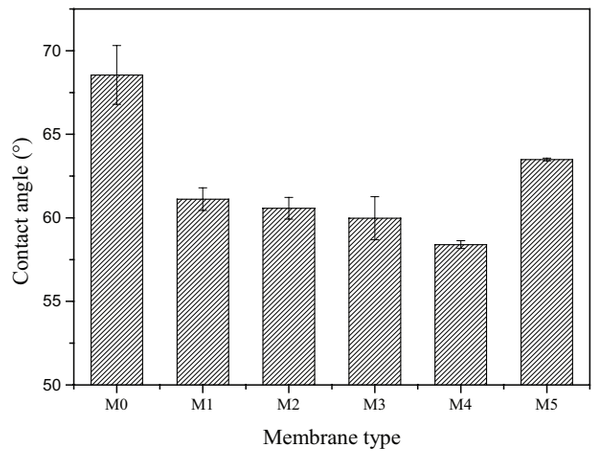

Fig. 8. Contact angle of the membranes.

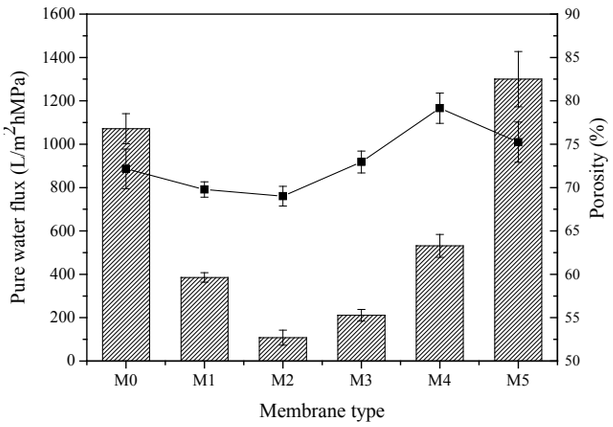

Fig. 9. Pure water flux and porosity of the prepared membranes.

the rejection rate is continuously increased from M1 to M3. However, it begins to decrease to some extent. According to Fig. 6 and BET analysis, the size of pores became smaller firstly and then larger due to the composition change. As a result, the number of BSA passed through the pores was decreased at first, which may lead to increased retention rate. Subsequently, with some larger pores formed, the number of passed BSA molecules was increased, which conversely led to decreased retention rate [43].

Employing BSA as a model foulant, the permeation flux decline and recovery were measured in a dead-end filtration module, which indicated the antifouling properties of the prepared membranes. Fig. 12 shows the time-dependent flux, reflecting the influence of MgSiO addition amount in PES membranes on the membrane properties mainly, and Table 5 gives the corresponding *FRR*, R_t, R_r and R_{ir} values. The flux recovery ratio (*FRR*) and total flux decline ratio (R_t) are the measure of antifouling property of the membranes. All MgSiO hybrid membranes showed higher *FRR* and lower R_t values than the PES membrane. The PES membrane exhibited poor antifouling properties: R_t and R_{ir} were as high as 70.2% and 47.8% respectively, and *FRR* as low as 52.2%. As the addition amount of MgSiO in the PES membrane was reached to M1, R_t and R_{ir} were decreased to 61.7% and 34.1%, respectively. Moreover, *FRR* of the membrane reached to 65.9%. As the addition amount of MgSiO in the PES membranes increasing, the antifouling parameter *FRR* of the prepared membranes was elevated up to the maximum values 84.3% (M2), and then decreased gradually. Because the weakened interaction force between membrane surface and BSA, caused by the increase in hydrophilic MgSiO, *FRR* value increased [30]. Furthermore, the addition of MgSiO changed the porosity of the membrane, shown in Fig. 9, which greatly altered the mass transfer resistance of membranes and of importance for antifouling properties [44]. However, with the MgSiO continued to increase, the antifouling properties were impaired somewhat, which might be ascribed to the increased roughness [45,46]. In comparison, the antifouling properties of the MgSiO hybrid membrane were overall enhanced.

Similarly, bovine serum albumin (BSA) was used as the model foulant to evaluate the protein resistance of the prepared membranes. The protein static adsorption study was carried out, and the adsorption amount of the membranes is demonstrated in Fig. 13. The BSA adsorption amount of PES membrane was 12.57 μg/cm². After modification, the BSA adsorption amount for MgSiO/PES membranes was firstly declined and then increased. The BSA adsorption amount of membrane M1 was 7.59 μg/cm². When MgSiO was increased to 4%, the BSA adsorption amount of membrane M2 was reduced to 4.62 μg/cm², and then gradually increased to 9.51 μg/cm². It could be concluded that in some way, the higher surface coverage of MgSiO, the less amount of BSA molecules adsorbed on membrane surface. However, it is believed that the surface roughness and specific surface area influence the membrane adsorption capacity [47,48]. Accordingly, the increased adsorption could be interpreted as the increased roughness and increased BET surface area. Meanwhile, it is believed that the membrane with high porosity gives more adsorption site, caused higher adsorption [48]. The results are basically in line with the antifouling experiments, the membrane with higher hydrophilicity and lower roughness possessed lower protein adsorption and stronger antifouling property.

3.7. MB (methylene blue) filtration experiments

The ultrafiltration experiments were carried out using 6 mg/L MB solution as feed solution. Fig. 14 manifests the rejection to MB solution at 0.1 Mpa as a function of time. After a 90 min filtration of MB solution, the membranes were

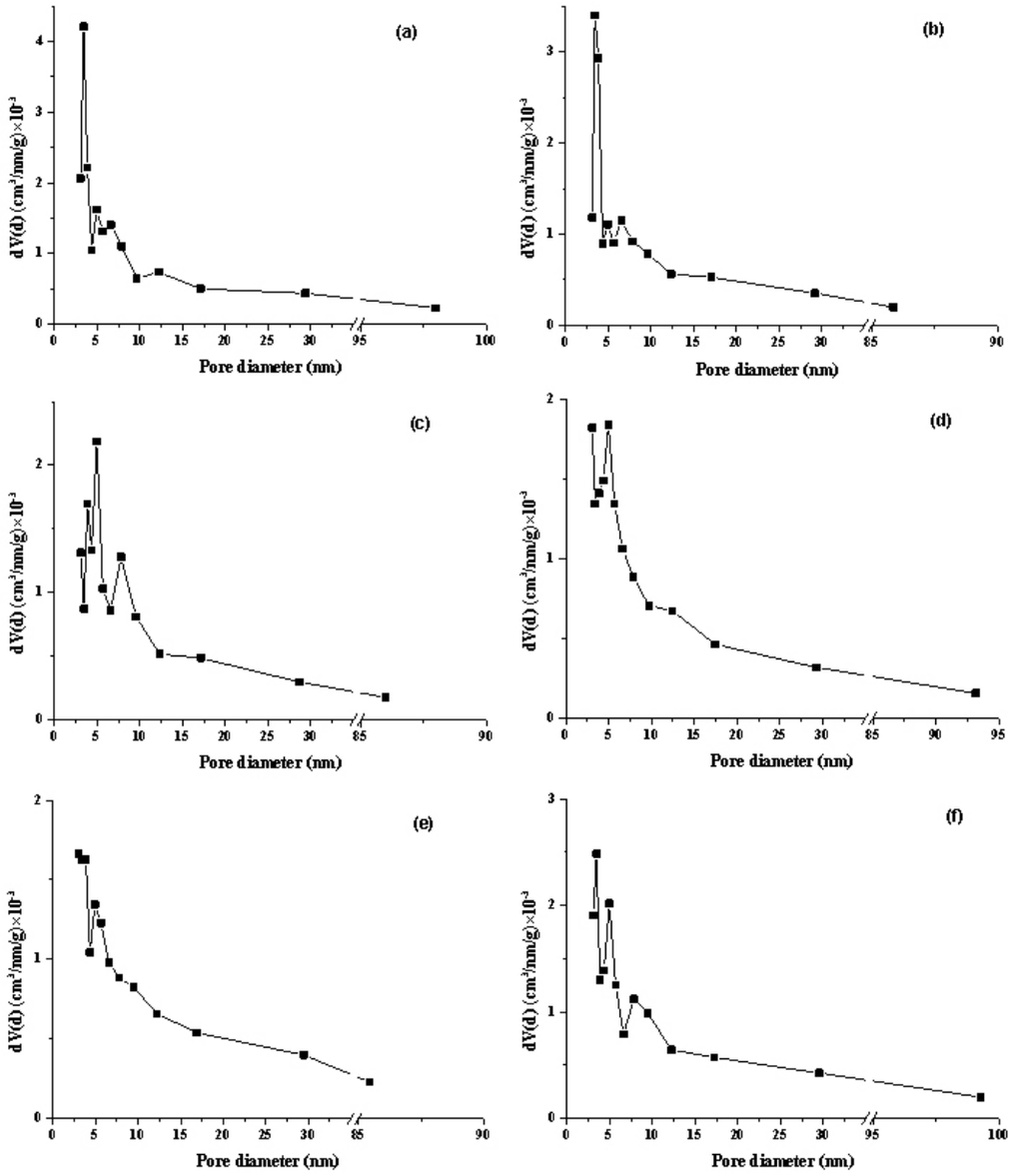

Fig. 10. Pore size distribution of the prepared membranes: (a–f) M0–M5.

Table 4
Experimental results obtained from BET analysis

Sample	Average pore diameter (nm)	BET surface area (m^2/g)
M0	11.83	18.81
M1	10.84	15.95
M2	9.35	17.47
M3	9.52	17.35
M4	10.53	17.93
M5	10.98	18.97

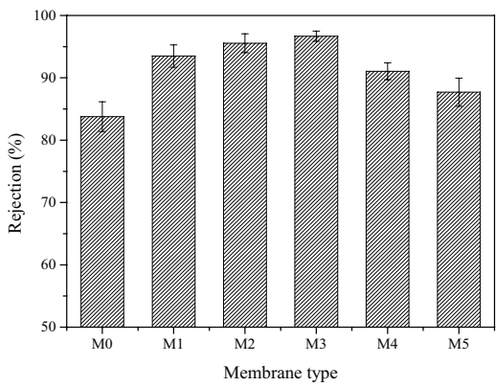

Fig. 11. BSA rejection of the prepared membranes.

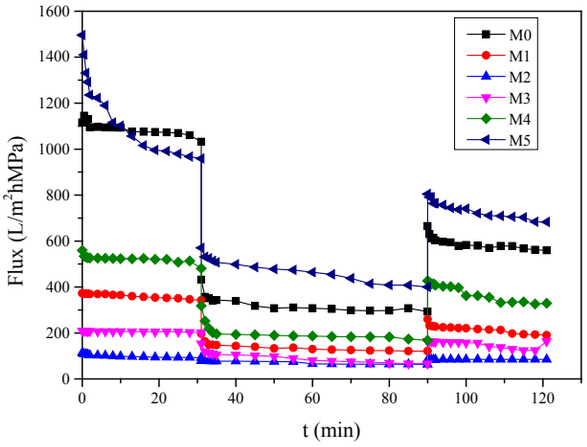

Fig. 12. Time-dependent flux of the membranes includes fouling and cleaning process.

Table 5
Antifouling parameters of the membranes for BSA filtration

Sample	*FRR*(%)	R_t(%)	R_r(%)	R_{ir}(%)
M0	52.2	70.2	22.4	47.8
M1	65.9	61.7	27.3	34.1
M2	84.3	28.7	12.9	15.7
M3	73.1	54.5	27.6	26.9
M4	71.9	61.6	33.6	28.1
M5	65.6	58.8	24.4	34.4

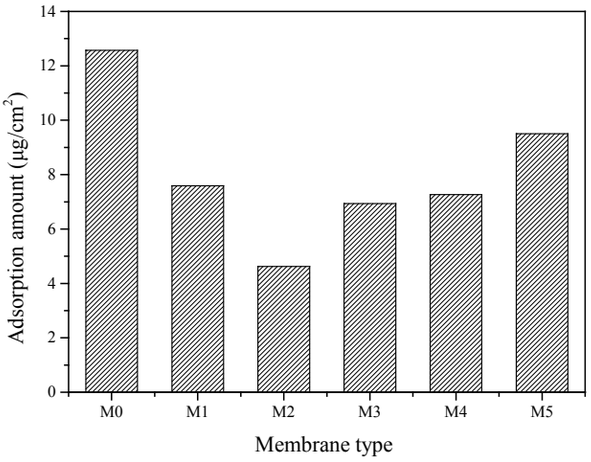

Fig. 13. BSA adsorptionamount of the prepared membranes.

taken out from the membrane cell, followed by immersed in DI water for one day, and then they were displayed in Fig. 15. It could be obviously seen that all the membranes with MgSiO gave higher rejection towards MB than the membrane without MgSiO, and the color was getting deepen from M0 to M5. That maybe because MgSiO has a high

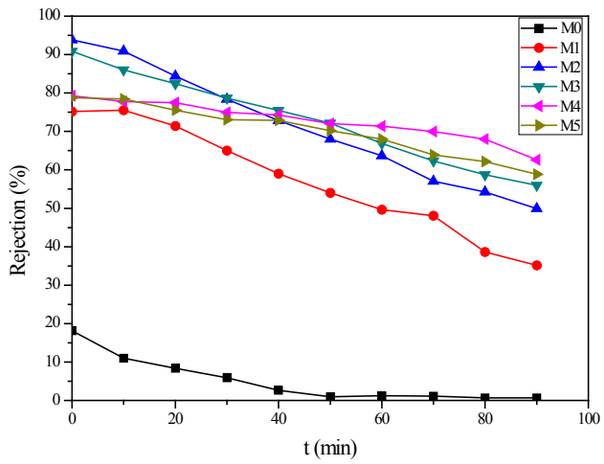

Fig. 14. Time-dependent rejection of methylene blue solution (6 mg/L).

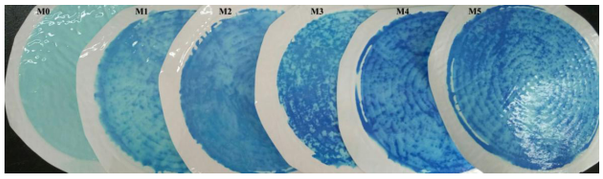

Fig. 15. Membranes after a certain time filtration of methylene blue solution.

adsorb tendency towards MB, when the filtrate permeate the membrane, MB can be adsorbed by MgSiO. At the beginning of filtration, the M2 presented the highest rejection, while at the end of filtration, M4 presented the highest, which might be attributed to the combined effect of permeability and the content of MgSiO. When the permeability is higher or the content of MgSiO is lower, MB cannot be adsorbed in no time. But the tendency in the sum of rejections for each membrane is consistent with the increase of MgSiO. However, all the rejections descend with time for the limited adsorbents, which is not satisfactory, so further filtration is still needed.

4. Conclusions

MgSiO/PES hybrid membranes were prepared by the previous reported in-situ synthesized phase inversion method. Compared with the PES membrane, the hydrophilicity and antifouling performance were basically enhanced due to the existence of MgSiO, and affected by the difference in concentration to some extent. The EDS, XRD and FT-IR results confirmed the effective formation of MgSiO in the hybrid membranes, and Mg/Si molar ratio is 1.36. Combined with SEM and BET results on pore structure, the existence of MgSiO changed pore width and specific surface area. Additionally, after the addition of certain amount of magnesium salt (M2), the more high percentage of MgSiO is,the larger membrane pore size becomes, which

is not contributed for the remove of macromolecular, but more efficient for methylene blue removal.

It is proved that homogeneous organic-inorganic hybrid membrane is accessible via in-situ synthesized phase inversion method, meanwhile, the magnesium silicate/polyethersulfone hybrid ultrafiltration membrane has high rejection on BSA molecular not only, but has effect on MB removal.

Acknowledgement

The present research was financially supported by Project 2014BAK13B02 supported by the National Science-technology Support Plan Projects.

References

[1] J. Chen, M. Liu, L. Zhang, J. Zhang, L. Jin, Application of nano TiO_2 towards polluted water treatment combined with electro-photochemical method, Water Res., 37 (2003) 3815–3820.
[2] J. Yeo, S.Y. Kim, S. Kim, D.Y. Ryu, T.H. Kim, Mechanically and structurally robust sulfonated block copolymer membranes for water purification applications, Nanotechnology, 23 (2012) 245703.
[3] M.N. Chong, B. Jin, C.W. Chow, C. Saint, Recent developments in photocatalytic water treatment technology: A review, Water Res., 44 (2010) 2997–3027.
[4] H.C. Duong, M. Duke, S. Gray, B. Nelemans, D.N. Long, Membrane distillation and membrane electrolysis of coal seam gas reverse osmosis brine for clean water extraction and NaOH production, Desalination, 397 (2016) 108–115.
[5] I. Ali, V.K. Gupta, Advances in water treatment by adsorption technology, Nat. Protoc., 1 (2006) 2661–2667.
[6] F. Ciesielczyk, P. Bartczak, K. Wieszczycka, K. Siwińska-Stefańska, M. Nowacka, T. Jesionowski, Adsorption of Ni(II) from model solutions using co-precipitated inorganic oxides, Adsorption, 19 (2013) 423–434.
[7] F. Ciesielczyk, P. Bartczak, T. Jesionowski, Removal of nickel(II) and cadmium(II) ions from aqueos solutions using an oxide adsorbent of MgO-SiO_2 type, Desal. Water Treat., 55 (2015) 1271–1284.
[8] F. Ciesielczyk, P. Bartczak, T. Jesionowski, Removal of cadmium(II) and lead(II) ions from model aqueous solutions using sol-gel-derived inorganic oxide adsorbent, Adsorption, 22 (2015) 445–458.
[9] F. Ciesielczyk, P. Bartczak, L. Klapiszewski, T. Jesionowski, Treatment of model and galvanic waste solutions of copper(II) ions using a lignin/inorganic oxide hybrid as an effective sorbent, J. Hazard. Mater., 328 (2017) 150–159.
[10] P. Palma, S. Fialho, P. Alvarenga, C. Santos, T. Brás, G. Palma, C. Cavaco, et al., Membranes technology used in water treatment: Chemical, microbiological and ecotoxicological analysis, Sci. Total Environ., 568 (2016) 998–1009.
[11] T. Peters, Membrane technology for water treatment, Chem. Eng. Technol., 33 (2010) 1233–1240.
[12] V. García, P. Häyrynen, J, Landaburu-Aguirre, M. Pirilä, R.L. Keiski, A. Urtiaga, Purification techniques for the recovery of valuable compounds from acid mine drainage and cyanide tailings: application of green engineering principles, J. Chem. Technol. Biot., 89 (2014) 803–813.
[13] S. Arefi-Oskoui, V. Vatanpour, A. Khataee, Development of a novel high-flux PVDF-based ultrafiltration membrane by embedding Mg-Al nanolayered double hydroxide, J. Ind. Eng. Chem., 41 (2016) 23–32.
[14] O. Lorain, B. Hersant, F. Persin, A. Grasmick, N. Brunard, J.M. Espenan, Ultrafiltration membrane pre-treatment benefits for reverse osmosis process in seawater desalting. Quantification in terms of capital investment cost and operating cost reduction, Desalination, 203 (2007) 277–285.
[15] H. Song, F. Ran, H. Fan, X. Niu, L. Kang, C. Zhao, Hemocompatibility and ultrafiltration performance of surface-functionalized polyethersulfone membrane by blending comb-like amphiphilic block copolymer, J. Membr. Sci., 471 (2014) 319–327.
[16] M. Baghbanzadeh, D. Rana, C.Q. Lan, T. Matsuura, Effects of inorganic nano-additives on properties and performance of polymeric membranes in water treatment, Sep. Purif. Rev., 45 (2016) 141–167.
[17] E. Celik, H. Park, H. Choi, H. Choi, Carbon nanotube blended polyethersulfone membranes for fouling control in water treatment, Water Res., 45 (2011) 274–282.
[18] Z. Xu, L. Yu, L. Han, Polymer-nanoinorganic particles composite membranes: a brief overview, Front. Chem. Eng. China, 3 (2009) 318–329.
[19] X. Liu, Y. Peng, S. Ji, A new method to prepare organic–inorganic hybrid membranes, Desalination, 221 (2008) 376-382.
[20] H.Q. Liang, Q.Y. Wu, L.S. Wan, X.J. Huang, Z.K. Xu, Thermally induced phase separation followed by in situ sol–gel process: A novel method for PVDF/SiO_2 hybrid membranes, J. Membr. Sci., 465 (2014) 56–67.
[21] S. Singh, A. Jasti, M. Kumar, V.K. Shahi, A green method for the preparation of highly stable organic-inorganic hybrid anion-exchange membranes in aqueous media for electrochemical processes, Polymer Chem., 8 (2010) 1302–1312.
[22] S. Han, L. Mao, T. Wu, H. Wang, Homogeneous polyethersulfone hybrid membranes prepared with in-situ synthesized magnesium hydroxide nanoparticles by phase inversion method, J. Membr. Sci., 516 (2016): 47–55.
[23] A.P. Mairal, J. Ly, A. Ng, I. Pinnau, Ultrafiltration Process: US, US20110100914. 2011.
[24] E. Arkhangelsky, A. Duek, V. Gitis, Maximal pore size in UF membranes, J. Membr. Sci., 394-395 (2012) 89–97.
[25] J.H. Huang, C.F. Zhou, G.M. Zeng, X. Li, J. Niu, et al., Micellar-enhanced ultrafiltration of methylene blue from dye wastewater via apolysulfone hollow fiber membrane, J. Membr. Sci., 365 (2010) 138–144.
[26] I. Rashid, N.H. Daraghmeh, M.M. Al Omari, B.Z. Chowdhry, S.A. Leharne, et al., Magnesium silicate, Profiles Drug Subst. Excip. Related Methodol., 36 (2011) 241–285.
[27] H. Yang, B. Sun, H. Wang, Removal of anionic dye from aqueous solution by magnesium silicate gel, Desal. Water Treat., 52 (2014) 7685–7692.
[28] Q. Lu, Q. Li, J. Zhang, J. Li, J. Lu, Facile mesoporous template-assisted hydrothermal synthesis of ordered mesoporous magnesium silicate as an efficient adsorbent, Appl. Surf. Sci., 360 (2016) 889–895.
[29] F. Ciesielczyk, P. Bartczak, J. Zdarta, T. Jesionowski, Active MgO-SiO_2 hybrid material for organic dye removal: A mechanism and interaction study of the adsorption of C.I. Acid Blue 29 and C.I. Basic Blue 9, J. Environ. Manage., 204 (2017) 123–135.
[30] Y. Liu, Y. Su, X. Zhao, Y. Li, R. Zhang, Z. Jiang, Improved antifouling properties of polyethersulfone membrane by blending the amphiphilic surface modifier with crosslinked hydrophobic segments, J. Membr. Sci., 486 (2015) 195–206.
[31] J. Zhang, L. Dang, M. Zhang, S. Zhao, Q. Lu, Micro/nanoscale magnesium silicate with hierarchical structure for removing dyes in water, Mater. Lett., 196 (2017) 194–197.
[32] D.R.M. Brew, F.P. Glasser, Synthesis and characterisation of magnesium silicate hydrate gels, Cem. Concr. Res., 35 (2005) 85–98.
[33] I.M. Ali, Y.H. Kotp, I.M. El-Naggar, Thermal stability, structural modifications and ion exchange properties of magnesium silicate, Desalination, 259 (2010) 228–234.
[34] J. Temuujin, K. Okada, K.J.D. Mac Kenzie, Role of water in the mechanochemical reactions of MgO-SiO_2 systems, J. Solid State Chem., 138 (1998) 169–177.
[35] T.W. Sun, Y.J. Zhu, C. Qi, F. Chen, Y.Y. Jiang, et. al., Templated solvothermal synthesis of magnesium silicate hollow nanospheres with ultrahigh specific surface area and their application in high-performance protein adsorption and drug delivery, J. Mater. Chem. B, 4 (2016) 3257–3268.

[36] Y. Zhang, Y. Li, Y. Xu, S. Sang, S. Jin, Enhanced formation of magnesium silica hydrates (M-S-H) using sodium metasilicate and caustic magnesia in magnesia castables, Ceram. Int., 43 (2017) 9110–9116.
[37] C. Dong, G. He, H. Li , R. Zhao, Y. Han, Y. Deng, Antifouling enhancement of poly (vinylidene fluoride) microfiltration membrane by adding $Mg(OH)_2$ nanoparticles, J. Membr. Sci., 387–388 (2012) 40–47.
[38] A. Sotto, A. Boromand, R. Zhang, P. Luis, J.M. Arsuaga, et. al., Effect of nanoparticle aggregation at low concentrations of TiO_2 on the hydrophilicity, morphology, and fouling resistance of PES-TiO_2 membranes. J. Colloid. Interf. Sci., 363 (2011) 540–550.
[39] M. Homayoonfal, A. Akbari, M.R. Mehrnia, Preparation of polysulfone nanofiltration membranes by UV-assisted grafting polymerization for water softening, Desalination, 263 (2010) 217–225.
[40] J.J. Bikerman, the surface roughness and contact angle, J. Phys. Chem., 54 (1950) 653–658.
[41] A.T. Kittu, R. Bulut, J. Puckette, Effects of surface roughness on contact angle measurements on a limestone aggregate, Geo-Hubei 2014 International Conference on Sustainable Civil Infrastructure, 2014.
[42] E. Saljoughi, M. Amirilargani, T. Mohammadi, Effect of PEG additive and coagulation bath temperature on the morphology, permeability and thermal/chemical stability of asymmetric CA membranes, Desalination, 262 (2010) 72–78.
[43] K.J. Hwang, P.Y. Sz, Effect of membrane pore size on the performance of cross-flow microfiltration of BSA/dextran mixtures, J. Membr. Sci., 378 (2011) 272–279.
[44] S. Zhao, W. Yan, M. Shi, Z. Wang, J. Wang, S. Wang, Improving permeability and antifouling performance of polyethersulfone ultrafiltration membrane by incorporation ofZnO-DMF dispersion containing nano-ZnO and polyvinylpyrrolidone, J. Membr. Sci., 478 (2015) 105–116.
[45] T.C. Ying, E. Mahmoudi, A.W. Mohammad, A. Benamor, D. Johnson, N. Hilal, Development of polysulfone-nanohybrid membranes using ZnO-GO composite for enhanced antifouling and antibacterial control, Desalination, 402 (2017) 123–132.
[46] Ho. Li, W. Shi, Q. Du, R. Zhou, H. Zhang, X. Qin, Improved separation and antifouling properties of thin-film composite nanofiltration membrane by the incorporation of cGO, Appl. Surf. Sci., 407 (2017) 260–275.
[47] M. Safarpour, V. Vatanpour, A. Khataee, Preparation and characterization of graphene oxide/TiO_2 blended PES nanofltration membrane with improved antifouling and separation performance, Desalination, 393 (2016) 65–78.
[48] K.M. Persson, G. Capannelli, A. Bottino, G. Trägrädh, Porosity and protein adsorption of four polymeric microfiltration membranes, J. Membr. Sci., 76 (1993) 61–71.